Sensors and Actuators A 193 (2013) 149–154

Contents lists available at SciVerse ScienceDirect

Sensors and Actuators A: Physical

journal homepage: www.elsevier.com/locate/sna

# Photonic crystal stress sensor with high sensitivity in double directions based on shoulder-coupled aslant nanocavity

Yi Yang[a,b], Daquan Yang[a,b], Huiping Tian[a,b], Yuefeng Ji[a,b,*]

[a] State Key Laboratory of Information Photonics and Optical Communications, Beijing 100876, China
[b] School of Information and Communication Engineering, Beijing University of Posts and Telecommunications, Beijing, China

ARTICLE INFO

*Article history:*
Received 18 October 2012
Received in revised form
22 December 2012
Accepted 21 January 2013
Available online 29 January 2013

*Keywords:*
Photonic crystals
Stress sensor
Nanocavity
Waveguide
SOI

ABSTRACT

In this paper, we demonstrate a photonic crystal (PhC) stress sensor with high sensitivity in two orthogonal directions. The stress sensor consists of an aslant lattice-shifted resonant cavity shoulder-coupled to two terminated $\Gamma$–$K$ waveguides. The linear relationship between the shifts of resonant wavelength and applied stress in double directions is calculated with the finite element method (FEM) and finite difference time domain (FDTD) simulations. With the simulations, we demonstrate that the stress sensitivity of 7.5 nm/μN in horizontal direction and 10 nm/μN in vertical direction is achieved, respectively, and a stress detection limit is approximately of 58 nN and 44 nN in horizontal and vertical direction for this device, respectively.



## 1. Introduction

In the past few decades, photonic crystal (PhC) has been attracting an increasing interest since Yablonovitch and John proposed in 1987, respectively [1,2]. PhC has wide photonic bandgap (PBG) and photon confinement ability; these optical characteristics have attracted more and more interest in the manufacturing optical devices. Lately, due to the robust characteristics such as small size, high sensitivity, accurate limit of detection and can be easily integrated, a variety of sensing applications have been investigated and developed by employing PhC structures. Sensors based on PhC have been designed for temperature sensing, biochemical sensing, humidity sensing and so on, as result of they are sensitive to tiny perturbation of the refractive index that corresponds to the surrounding temperature [3], the bounding of biochemical molecules [4–6], or humidity around [7]. Most of such PhC structures consist of relatively low-loss waveguides [8] and nanocavities with high quality factor [6,9], which are favorable for superminiature integrated sensor applications.

Besides, mechanical sensing by using PhC structures has also been studied so far [10–15]. For example, Yang et al. carried out a microdisplacement sensor based on slot PhC structure with high Q factor cavity that utilizes the intensity of transmittance spectra as a token of the displacement [10], Lu et al. proposed a stress sensor based on the changes of optical properties caused by the variation of double-layered photonic crystal microcavity [11] and Lee et al. proposed stress sensors with high sensitivity based on PhC which measure changes in the resonant frequency in transmittance spectra when forces were applied on the cantilever [12–14]. In addition, Winger et al. presented a nanocavity with electromechanical and optomechanical characteristics, which combined with an electrical circuit with a high quality factor PhC nanocavity to realize electrokinetic sensor [15]. However, in these studies, the generated stress on these measurements were just taken along in one direction [12,13], stress sensors operated in multiplex directions were not studied.

In our paper, we demonstrate a stress sensor with a high quality factor aslant nanocavity that makes it possible to achieve high sensitivity in both the horizontal and vertical direction. The cavity we designed is 60° from $\Gamma$–$K$ direction so that the applied stress in both directions generated almost the same geometry variations on the cavity. With this stress sensor fixed on the base, we can detect the stress from two orthogonal directions which is important in multidirectional and reusable stress sensing. In order to leak the light inside the cavity onto the output waveguide for detecting the resonant wavelength in transmittance spectra, the cavity is shoulder-coupled [16] by two symmetrical W1 waveguides to acquire a stronger coupling strength. Firstly, with the FEM simulation, we obtain the variations of air holes caused by the applied stress. Then the structure variations lead to the shift of the resonant

* Corresponding author at: P.O. Box 90, BUPT, No. 10, Xitucheng Road, Haidian District, Beijing 100876, China.
*E-mail address:* jyf@bupt.edu.cn (Y. Ji).

0924-4247/$ – see front matter © 2013 Elsevier B.V. All rights reserved.
http://dx.doi.org/10.1016/j.sna.2013.01.045

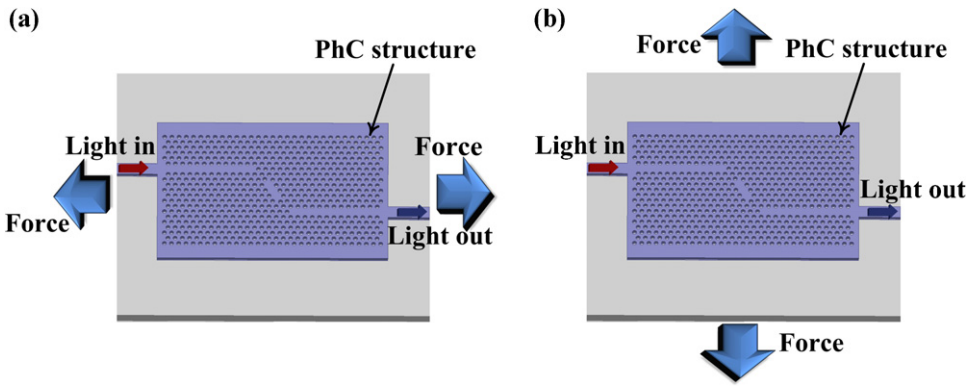


**Fig. 1.** Schematic of the stress sensor design under stress in horizontal direction (a) and vertical direction (b).

wavelength, the shift of output resonant peak was calculated by 3D FDTD simulation. Ultimately, by utilizing FEM and 3D FDTD simulations together, the sensitivity of 7.5 nm/μN in horizontal direction and 10 nm/μN in vertical direction is obtained, respectively, and a stress detection limit is approximately of 58 nN and 44 nN in horizontal and vertical direction for this device.

## 2. Stress sensor design principle

### 2.1. Stress sensing principle

Fig. 1 presents a schematic of the stress sensor design based on a piece of Si PhC structure. There are two waveguides and one aslant cavity created on the structure by removing or shifting the air holes. The geometries and positions of the air holes were modified by applying mechanical force on the structure. The stress sensing can be realized from the measurement of change in the optical property.

There are two ways to detect the stress by measuring the change of optical properties. The first one is paying attention to measuring the variation of intensity in transmittance spectra. The other one is by observing the shift of specific wavelength. However, we choose the latter one in this case because many factors may impact the intensity and cause errors. Here we choose the resonant wavelength of the aslant cavity as the candidate and observe its shift to deduce the applied force. The direction of stress can be differentiated by detecting the resonant wavelength has a red shift or a blue shift. And the value of stress can be known by measuring the displacement of the resonant wavelength. By utilizing FEM and 3D FDTD simulations together, we could estimate the force by measuring the shift of resonant wavelength and calculate the sensitivity ($S$, defined as resonant wavelength shift in nanometer per stain variation in micro Newton unit, that is, nm/μN) of this stress sensing structure. Eq. (1) is defined to illustrate this relationship:

$$S = \frac{\Delta\lambda}{\Delta F} \tag{1}$$

where $\Delta\lambda/\Delta F$ represents the resonant wavelength shift caused by the specific applied force. With the high Q factor cavity we can achieve large $\Delta\lambda/\Delta F$, that is, larger shift of resonant wavelength on the condition that fixed stress has been set. Then the stress detect limit can be defined ($L$, in nano Newton unit) with the line-width of the resonant peak, which is equal to the quality factor. Thus Eq. (1) can be modified to:

$$L = \frac{\Delta F}{\Delta\lambda} \times \frac{\lambda}{Q} = \frac{\lambda}{SQ} \tag{2}$$

where, $\lambda$, $Q$, and $\lambda/Q$ represent the resonant wavelength of the cavity, the quality factor, and the line-width of the resonant peak, respectively. Consequently, the detect limit $L$ is influenced by two significant parameters: $S$ and $Q$. When the sensitivity is fixed, we can achieve small $L$ with this high quality aslant cavity in horizontal direction (Fig. 1(a)) and vertical direction (Fig. 1(b)). The nonlinear effect such as Kerr effect can also change the refractive index of Si. However, according to Ref. [17], when the injected light power is not too high, the variation of refractive index is ultra-small. When the input power was 60 μW, the refractive index changed $0.5 \times 10^{-4}$ and we found that the resonant wavelength shifted only $6.239 \times 10^{-4}$ nm. It is really small to affect the sensing property.

### 2.2. PhC structure design

In the past few decades, PhC cavity structures have been drawing much attention for its small mode volume and ability to strongly confine light. Many studies have focused on putting forward various cavities [18,19] and optimizing the cavities geometry [20,21]. But these cavities are almost constructed parallel to the direction of light propagation so that insensitive to the stress applied in other directions except the direction along the cavity. In order to obtain robust sensing performance in both directions, we present an aslant cavity to achieve the goal.

The detail of the PhC structure has been shown in Fig. 2, as the PhC structure is the key component of the stress sensor and play a crucial role in the stress sensing sensitivity. Particularly, the aslant cavity is the core of the PhC structure because the performance of the cavity influences the property of the whole sensor. Triangular lattice design are structured in a silicon slab ($n_{si} = 3.48$) with air holes, where the two air holes (in the direction 60° from $\Gamma$–$K$ direction) are shifted from the original lattice positions and the three air holes between them are filled to construct an aslant cavity. In this

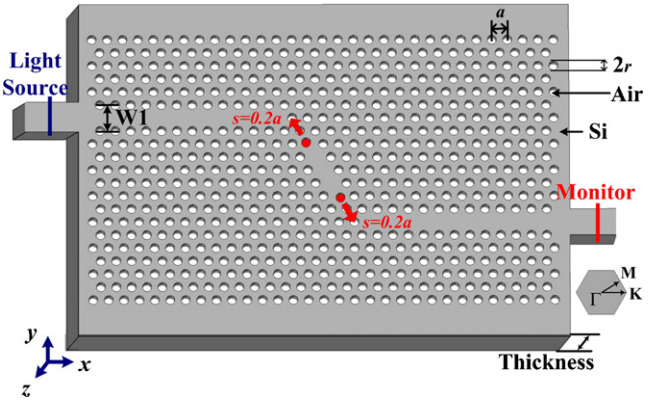


**Fig. 2.** 3D schematic of the PhC structure, where lattice constant $a = 385$ nm, diameter of air holes $d = 0.6a$, thickness $t = 0.56a$, shift of holes $s = 0.2a$, refractive index of Si $n_{si} = 3.48$.

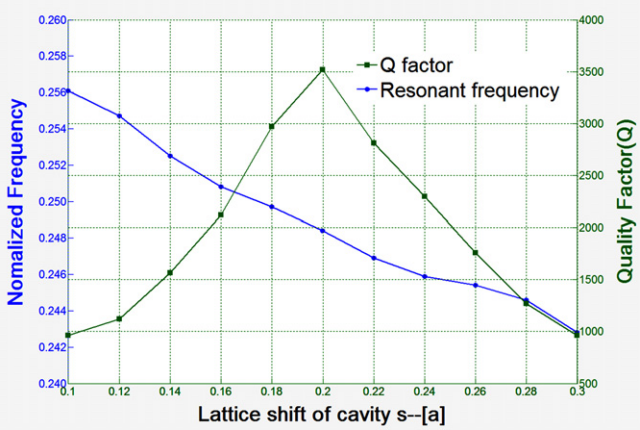


**Fig. 3.** The variation trend of the aslant cavity resonant frequency and quality factor with the change of $s$, the lattice shift along the direction which is 60° from $\Gamma$–$K$ direction.

paper, open source 3D FDTD simulation software Meep [22] was used to analyze the transmittance spectra. Light source was placed at the head of the input W1 waveguide and monitor was placed at the end of the output W1 waveguide. Transmittance spectra were calculated by dividing the output power detected with the monitor by the input power of the source. We set the resolution of Meep to 20 (namely, with a spatial grid size of $a/20$, where $a$ is the lattice constant) and the temporal time steps of 50 time units (about 13 periods) in all of our simulations to ensure the results obtained with same accuracy.

Fig. 2 shows the aslant cavity is shoulder-coupled between two W1 waveguides and the PhC structure is centro-symmetric in top view. The input W1 waveguide is placed three rows of air holes above the cavity and the output W1 waveguide is placed three rows of air holes below the cavity. Air holes in the W1 waveguides are removed until the hole along the direction of aslant cavity to achieve the best coupling strength. The careful design at the corner ensures the excellent coupling strength and reduces the loss between W1 waveguide and the cavity compared to other kinds of coupling structures such as butt-coupled structure and side-coupled structure in Refs. [16,23,24]. From the transmittance spectra in Fig. 4(b) we can see the peak we used reaches 0.9, the total coupling loss is small. The lattice constant of the PhC is $a = 385$ nm. All of the air holes have the same diameter of $d = 0.6a = 231$ nm. The photonic crystal slab's thickness is $t = 0.56a = 215.6$ nm. We designed an aslant cavity which three air holes are defected in the direction 60° from $\Gamma$–$K$ direction and the outer holes of the cavity are shifted outwards along the oblique line. We used Meep to design and optimize the cavity so that two main optical characteristics are taken to be considered: resonant frequency and quality factor. The length of the cavity is crucial to the optical characteristics and we adjust the air holes to fit the length. We defined the shift of each outer hole outwards away from the original position is $s$ (in nanometer unit). The shift s increased from $0.1a$ to $0.3a$ with an increment of $0.02a$ and all the structures were simulated by discovering the variation rules of the optical characteristics. Fig. 3 presents the variation tendency of the resonance frequency and quality factor with the change of the shift. From Fig. 3 we observe the resonant frequency decreases from $0.2561(2\pi c/a)$ to $0.2428(2\pi c/a)$ when the hole shift increases, which means that the resonant wavelength has a red shift. This is because the larger shift of lattice provides more high-dielectric region inside the cavity. But the highest quality factor is obtained when $s = 0.2a$ and the peak value is 3500 because of the maximum overlap is achieved in this structure. Therefore, we employed the cavity with $s = 0.2a$ as our final cavity structure in the stress sensor.

A narrow band TE-like polarization light source was placed at the center of the cavity to simulate the electric field distribution without applied stress. The dark red and blue regions showed in Fig. 4(a) represent the aslant cavity has great ability in confining light. Slight variation of the air holes around the cavity changes the structure of the cavity and shifts the resonant wavelength. According to Eq. (2), highly sensitive stress senor can be easily achieved based on this high quality cavity. With a Gaussian-pulse source placed in front of the input waveguide in Fig. 2, transmittance spectra can be monitored at the end of output waveguide. The transmittance spectra of original PhC structure are shown in Fig. 4(b) after data processing (where data processing represents dividing the output power detected with the monitor by the input power of the source). The result in Fig. 4(b) shows four peaks at $0.2124(2\pi c/a)$, $0.2258(2\pi c/a)$, $0.2484(2\pi c/a)$, and $0.2674(2\pi c/a)$, respectively. We choose the resonant frequency of $0.2484(2\pi c/a)$ to observe the shift of its corresponding resonant wavelength ($\lambda_c = 1549.9$ nm) when force is applied.

## 3. FEM simulation of structural variation under elastic stress

In this part, commercial FEM software ANSYS™ 13.0 was used to explore the variations of air holes caused by the applied stress. A 3D solid model was built by using physical parameters of Si so we used 169 GPa for Young's modulus and 0.28 for Poisson's ratio. The material of the model was assumed to be linear, elastic and isotropic. We used the model with the same geometry as the PhC structure designed before and all the parameters were set as mentioned in Section 2. The intermediate part of PhC structure was suspended and different value of static forces were applied on the ends in each direction. The deformation of PhC structure under different applied forces were all solved every substep.

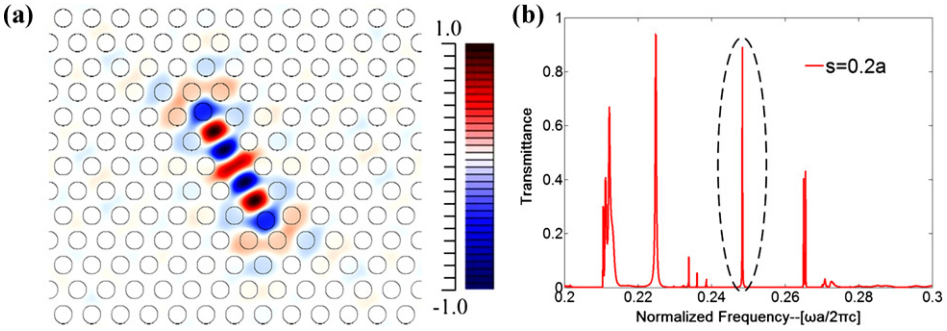


**Fig. 4.** (a) Electric field distribution in $x$–$y$ plane of the aslant cavity by using 3D FDTD simulations; (b) transmittance spectra of original PhC structure which shows four peaks at $0.2124(2\pi c/a)$, $0.2258(2\pi c/a)$, $0.2484(2\pi c/a)$, and $0.2674(2\pi c/a)$.

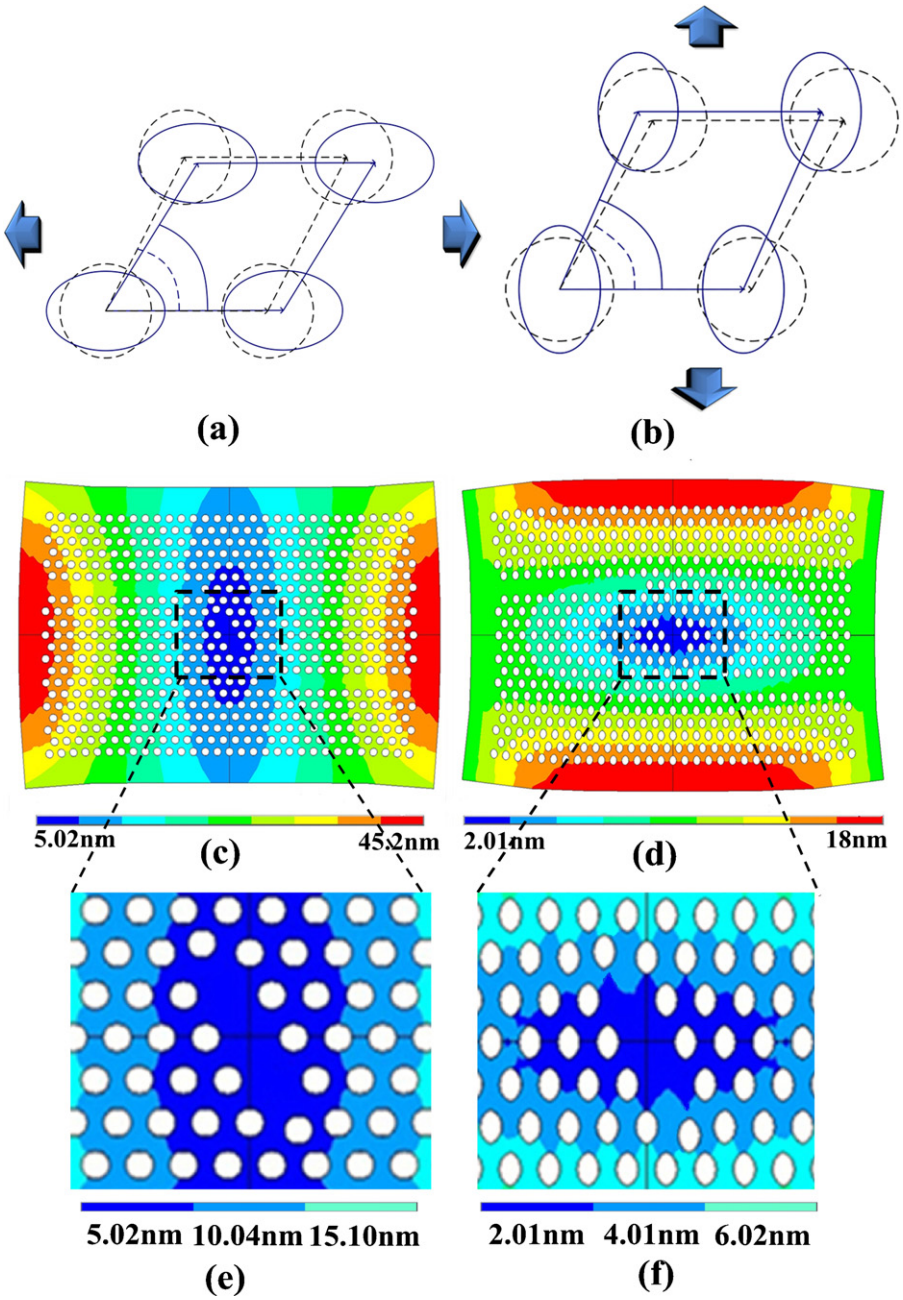


**Fig. 5.** Schematic of air holes' variations under stress in horizontal direction (a) and vertical direction (b). Deformation contour plot of the model under −1 μN force load in horizontal direction (c) and vertical direction (d). (e) and (f) are the details of the cavity area.

We simulated the structural variation under force, where the force ($F$, in micro Newton unit) considered were 0.25 μN, −0.25 μN, 0.5 μN, −0.5 μN, 0.75 μN, −0.75 μN, 1 μN, and −1 μN (the $F$ means squeeze and the $-F$ means pull). Both horizontal direction and vertical direction were loaded respectively to see the variations of air holes. Fig. 5(a) and (b) clearly shows that air holes are relocated and distorted. Fig. 5(c) and (d) shows the deformed PhC structure contour plot of displacement vector sum with the strain force of −1 μN in two directions, respectively. They obviously show the displacement vector sum of each point on the PhC structure in $x$–$y$ plane. According to FEM simulations, the thickness of Si slab changed a little when the maximum force in our design was applied in double directions. With FDTD simulations we have found that the quality factor was slightly changed under such variation of thickness. The relationships among the applied force $F$, the changed thickness $\Delta t$ and the changed quality factor $\Delta Q$ are shown in Table 1. Therefore

**Table 1**
The relationships among the applied force $F$, the changed thickness $\Delta t$ and the changed quality factor $\Delta Q$.

| Direction | Horizontal | | Vertical | |
|---|---|---|---|---|
| $F$ | 1.0 μN | −1.0 μN | 1.0 μN | −1.0 μN |
| $\Delta t$ | $7.08 \times 10^{-11}$ m | $-7.08 \times 10^{-11}$ m | $5.98 \times 10^{-11}$ m | $-5.98 \times 10^{-11}$ m |
| $\Delta Q$ | −20 | −15 | −10 | −20 |

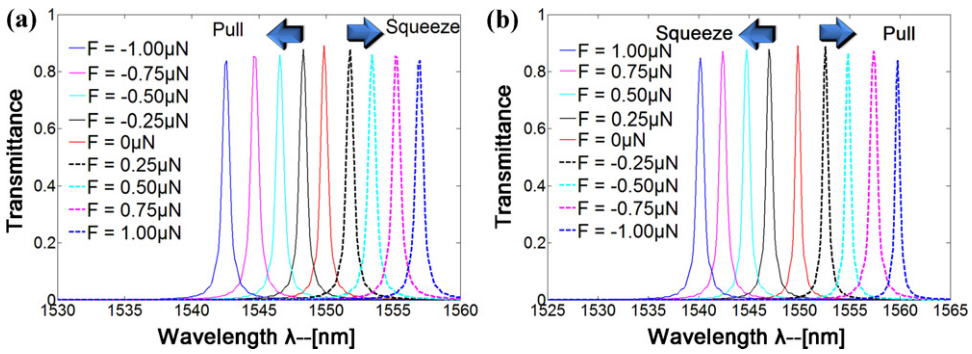


**Fig. 6.** Transmittance spectra showing the shift of resonant wavelength under different force in horizontal direction (a) and vertical direction (b).

the deformation in $z$ direction can be ignored because the slab is ultrathin. Later, such data of positions and shapes were put into the 3D FDTD software for subsequent simulations.

## 4. FDTD simulation and sensing characteristics discussion

All the different shapes of PhC structure under different applied stress were modeled in 3D FDTD software to obtain the transmittance spectra. Fig. 6 shows the transmittance spectra under different force from −1.00 μN to 1.00 μN in horizontal and vertical direction. The process to obtain transmittance spectra is the same as mentioned in Section 2 so that consistent comparison results are achieved.

From Fig. 6(a) and (b), we can see the shift of the resonant wavelength under force in double directions and the peaks are evenly distributed when the force varies from −1.00 μN to 1.00 μN. The resonant wavelength has a blue shift when the structure is pulled and a red shift when the structure is squeezed in horizontal direction. On the contrary, opposite results are obtained in vertical direction, which a blue shift is happened when squeezed and a red shift is happened when pulled. Therefore, when the structure was pulled we can differentiate the force from two directions by observing the shift direction of resonant wavelength. Similarly, when the structure was squeezed we can differentiate the direction of force in this way. We also find the intensity of the peak is pushed down a little when the force becomes bigger. This decay is mainly aroused by the modification of air holes around the cavity and the structure of cavity is slightly changed. Moreover, the reduction of intensity is related to the variation of the coupling waveguides. With the results from FEM and 3D FDTD simulations plugging into Eq. (1), the sensitivity is calculated to be 7.5 nm/μN and 10 nm/μN in the horizontal and vertical direction, respectively. Furthermore, with Eq. (2) and the simulations, the smallest $L$ we can obtain is 58 nN and 44 nN in the horizontal and vertical direction, respectively. Linear relationship between stress and shift of resonant wavelength has been achieved in the interval of our research. The results and linear relationship indicate it is a feasible way to sensing stress with this aslant cavity design. Fig. 7 shows the simulation results for the relationship between $\Delta\lambda$ (shift of resonant wavelength) and applied force $F$. From Fig. 7 we can discover the shifts in double directions are at the same level so that this aslant cavity design can minish the anisotropic property of traditional stress sensors and provide much convenience for integration of sensor array. This achievement is owed to the tilted cavity placed between the two mutually perpendicular stress directions. Whether the horizontal or vertical stress is applied, the variations of cavity length are almost the same so that the shifts of wavelength are almost the same. Therefore, sensitivity at the same level has been achieved in two directions.

Because both of the sensitivity $S$ and the detect limit $L$ are determined by the quality factor of the cavity, by using other ultra-high Q factor cavities [25,26] to replace the cavity in this structure can meet different demand at any level of $S$ and $L$. As the isotropy and small volume of this device, it allows us to form a stress sensor array by integrating numerous of these aslant cavities on one substrate. Therefore, with further work on this high quality factor cavity, stress sensors with higher sensitivity and stress sensor arrays with ultra-low limit of detection will come true.

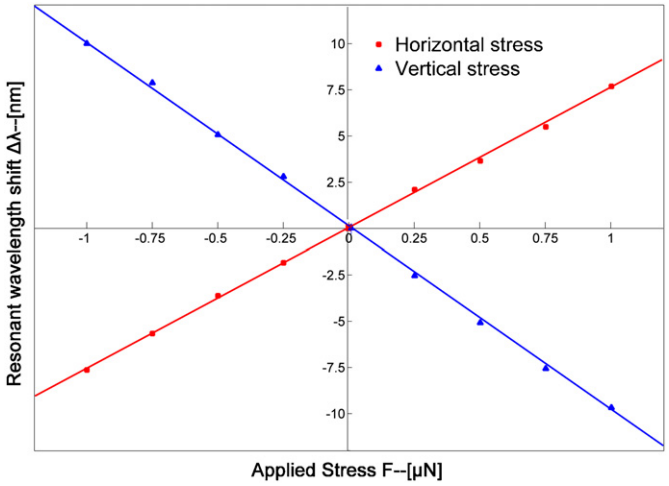


**Fig. 7.** Resonant wavelength shift vs. force in double directions.

## 5. Conclusion

In our paper, we have demonstrated a photonic crystal stress sensor based on one aslant nanocavity with high quality factor and two PhC waveguides. Highly sensitive stress sensing performance in double directions has been achieved. The aslant cavity is designed and optimized by shifting the air holes outwards in the direction 60° from $\Gamma$–$K$ direction with 3D FDTD simulations. The highest $Q$ = 3500 at corresponding wavelength $\lambda$ = 1549.9 nm is achieved when the shift $s = 0.2a$. According to the simulation results of FEM and 3D FDTD, we have demonstrated that the sensitivity of 7.5 nm/μN and 10 nm/μN in the horizontal and vertical direction is achieved, respectively. The relationship between stress and shift of resonant wavelength is linear in the interval of our research. Furthermore, the minimum detectable stress variation is 58 nN and 44 nN in the horizontal and vertical direction, respectively. The proposed aslant cavity is also hopeful in constructing optical stress sensor array for its super small volume and ultra-high sensitivity in double directions. In addition, the sensitivity of this stress sensor can be enhanced by optimizing the geometry of cavity to improve the quality factor.

## Acknowledgements

This research was supported in part by National 973 Program (No. 2012CB315705), National 863 Program (No. 2011AA010303, 2011AA010305, 2011AA010306), PR China.

## References

[1] E. Yablonovitch, Inhibited spontaneous emission in solid-state physics and electronics, Physical Review Letters 58 (20) (1987) 2059–2062.
[2] S. John, Strong localization of photons in certain disordered dielectric superlattices, Physical Review Letters 58 (23) (1987) 2486–2489.
[3] M.T. Tinker, J.-B. Lee, Thermo-optic photonic crystal light modulator, Applied Physics Letters 86 (22) (2005) 1797–1803.
[4] S. Kita, S. Hachuda, S. Otsuka, T. Endo, Y. Imai, Y. Nishijima, H. Misawa, T. Baba, Super-sensitivity in label-free protein sensing using a nanoslot nanolaser, Optics Express 19 (18) (2011) 17683–17690.
[5] S. Pal, E. Guillermain, R. Sriram, B.L. Miller, P.M. Fauchet, Silicon photonic crystal nanocavity-coupled waveguides for error-corrected optical biosensing, Biosensors and Bioelectronics 26 (10) (2011) 4024–4031.
[6] W. Lai, S. Chakravarty, Y. Zou, R.T. Chen, Silicon nano-membrane based photonic crystal microcavities for high sensitivity bio-sensing, Optics Letters 37 (7) (2012) 1208–1210.
[7] I.G. Kolobov, W.B. Euler, I.A. Levitsky, Optical humidity sensing and ultrasound effect for mesoporous silicon one-dimensional photonic crystals, Applied Optics 49 (1) (2010) 137–141.
[8] S.-Y. Lin, E. Chow, V. Hietala, P.R. Villeneuve, J.D. Joannopoulos, Experimental demonstration of guiding and bending of electromagnetic waves in a photonic crystal, Science 282 (5387) (1998) 274–276.
[9] Y. Akahane, T. Asano, B.-S. Song, S. Noda, High-Q photonic nanocavity in a two-dimensional photonic crystal, Nature 425 (6961) (2003) 944–947.
[10] D. Yang, H. Tian, Y. Ji, Micro displacement sensor based on high-Q nanocavity in slot photonic crystal, Optical Engineering 50 (5) (2011), 054402.
[11] T.W. Lu, P.T. Lee, Ultra-high sensitivity optical stress sensor based on double-layered photonic crystal microcavity, Optics Express 17 (3) (2009) 1518–1526.
[12] C. Lee, J. Thillaigovindan, Optical nanomechanical sensor using a silicon photonic crystal cantilever embedded with a nanocavity resonator, Applied Optics 48 (10) (2009) 1797–1803.
[13] B. Li, F.-L. Hsiao, C. Lee, Configuration analysis of sensing element for photonic crystal based NEMS cantilever using dual nano-ring resonator, Sensors and Actuators A: Physical 169 (2) (2011) 352–361.
[14] B.T. Tung, D.V. Dao, T. Ikeda, Y. Kanamori, K. Hane, S. Sugiyama, Investigation of stress sensing effect in modified single-defect photonic crystal nanocavity, Optics Express 19 (9) (2011) 1882–8829.
[15] M. Winger, T.D. Blasius, T.P.M. Alegre, A.H. Safavi-Naeini, S. Meenehan, J. Cohen, S. Stobbe, O. Painter, A chip-scale integrated cavity-electro-optomechanics platform, Optics Express 19 (25) (2011) 24905–24921.
[16] G.-H. Kim, Y.-H. Lee, Coupling of small, low-loss hexapole mode with photonic crystal slab waveguide mode, Optics Express 12 (26) (2004) 6624–6631.
[17] T. Uesugi, B.S. Song, T. Asano, S. Noda, Investigation of optical nonlinearities in an ultra-high-Q Si nanocavity in a two-dimensional photonic crystal slab, Optics Express 14 (1) (2005) 377–386.
[18] Z. Han, X. Checoury, L.-D. Haret, P. Boucaud, High quality factor in two-dimensional photonic crystal cavity on silicon-on-insulator, Optics Letters 36 (10) (2011) 1749–1751.
[19] S. Tomljenovic-Hanic, A. Rahmani, M.J. Steel, C.M. de Sterke, Comparison of the sensitivity of air and dielectric modes in photonic crystal slab sensors, Optics Express 17 (17) (2009) 14522–14557.
[20] C. Kang, C.T. Phare, Y.A. Vlasov, S. Assefa, S.M. Weiss, Photonic crystal slab sensor with enhanced surface area, Optics Express 18 (26) (2010) 27930–27937.
[21] D. Yang, H. Tian, Y. Ji, Nanoscale photonic crystal sensor arrays on monolithic substrates using side-coupled resonant cavity arrays, Optics Express 19 (21) (2011) 20023–20034.
[22] http://ab-initio.mit.edu/wiki/index.php/Meep
[23] A. Benmerkhi, M. Bouchemat, T. Bouchemat, N. Paraire, Numerical optimization of high-Q-factor photonic crystal microcavities with a graded air lattice, Journal of the Optical Society of America B: Optical Physics 28 (2) (2011) 336–341.
[24] D. Yang, H. Tian, Y. Ji, The properties of lattice-shifted microcavity in photonic crystal slab and its applications for electro-optical sensor, Sensors and Actuators A: Physical 171 (2011) 146–151.
[25] Y. Tanaka, T. Asano, S Noda, Design of photonic crystal nanocavity with Q-factor of similar to $10^9$, IEEE Journal of Lightwave Technology 26 (9–12) (2008) 1532–1539.
[26] M. Notomi, Manipulating light with strongly modulated photonic crystals, Reports on Progress in Physics 73 (9) (2010), 096501.

## Biographies

**Yi Yang** received the Bachelor's degree of Electronic Information Engineering from Beijing University of Posts and Telecommunications (BUPT) in 2011. He currently is a master candidate in the State Key Laboratory of Information Photonics and Optical Communications, Beijing University of Posts and Telecommunications (BUPT), Beijing, PR China. His research now focuses on the area of photonic crystals and sensors.

**Daquan Yang** received the Bachelor's degree of Electronic Information Science and Technology from JiNan University in 2009. He currently is a Ph.D. candidate in the State Key Laboratory of Information Photonics and Optical Communications, Beijing University of Posts and Telecommunications (BUPT), Beijing, PR China. His research now focuses on the area of photonic crystals and optical communication.

**Huiping Tian** received the B.S. and Ph.D. degrees from Shanxi University, Shanxi, China, in 1998 and 2003, respectively. Now she is an associate professor in the School of Information and Communication Engineering, Beijing University of Posts and Telecommunications (BUPT), Beijing, PR China. Her research interests are focused on the area of ultra-short and ultra-fast process in the transmission of optics, photonic crystals and broadband information networking.

**Yuefeng Ji** received the Ph.D. degree from Beijing University of Posts and Telecommunications (BUPT), Beijing, PR China. Now he is a professor in BUPT. His research interests are primarily in the area of broadband communication networks and optical communications, with emphasis on key theory, realization of technology and applications.